

Comparison of Porous Iron Trimesates Basolite F300 and MIL-100(Fe) As Heterogeneous Catalysts for Lewis Acid and Oxidation Reactions: Roles of Structural Defects and Stability

Amarajothi Dhakshinamoorthy,[†] Mercedes Alvaro,[†] Patricia Horcajada,[‡] Emma Gibson,[§] Muthusamy Vishnuvarthan,[§] Alexandre Vimont,[§] Jean-Marc Grenèche,[⊥] Christian Serre,[‡] Marco Daturi,[§] and Hermenegildo Garcia^{†,*}

[†]Instituto Universitario de Tecnología Química CSIC-UPV, Universidad Politécnica de Valencia, 46022 Valencia, Spain

[‡]Institut Lavoisier, UMR 8180 CNRS, Université de Versailles Saint Quentin en Yvelines, 78035 Versailles, France

[§]Laboratoire Catalyse et Spectrochimie, ENSICAEN, Université de Caen, CNRS, 6 Bd Maréchal Juin, F-14050 Caen, France

[⊥]Institut des Molécules et Matériaux du Mans, IMMM UMR CNRS 6283, LUNAM Université du Maine, 72085 Le Mans Cedex, France

S Supporting Information

ABSTRACT: Two porous iron trimesates, namely, commercial Basolite F300 (Fe(BTC); BTC = 1,3,5-benzenetricarboxylate) with unknown structure and synthetic MIL-100(Fe) (MIL stands for Material of Institut Lavoisier) of well-defined crystalline structure, have been compared as heterogeneous catalysts for four different reactions. It was found that while for catalytic processes requiring strong Lewis acid sites, Fe(BTC) performs better, MIL-100(Fe) is the preferred catalyst for oxidation reactions. These catalytic results have been rationalized by a combined *in situ* infrared and ⁵⁷Fe Mössbauer spectroscopic characterization. It is proposed that the presence of extra Brønsted acid sites on the Fe(BTC) and the easier redox behavior of the MIL-100(Fe) could explain these comparative catalytic performances. The results illustrate the importance of structural defects (presence of weak Brønsted acid sites) and structural stability (MIL-100(Fe) is stable upon annealing at 280 °C despite Fe³⁺-to-Fe²⁺ reduction) on the catalytic activity of these two solids, depending on the reaction type.

KEYWORDS: heterogeneous catalysis, metal organic frameworks, Lewis acid solids, aerobic oxidations



INTRODUCTION

There is much current interest in exploiting the properties of metal organic frameworks (MOFs) in heterogeneous catalysis.^{1–6} Porous MOFs are crystalline hybrid solids built up from inorganic subunits (metal ions or clusters) and organic linkers bearing several complexing groups (carboxylates, phosphonates, imidazolates, etc.).^{5,7–10} Their easily tunable topology and composition, with sometimes high content of unsaturated metal sites, combined with their high porosity ($V_p \sim 0.2–3 \text{ cm}^3 \text{ g}^{-1}$, $S_{\text{BET}} \sim 200–6000 \text{ m}^2 \text{ g}^{-1}$, $\text{Ø} \sim 2–50 \text{ Å}$) make these solids attractive candidates for heterogeneous catalysis, complementing other porous solids, such as zeolites and mesoporous metal oxides.¹¹

One of the key points to expand the use of MOFs as solid catalysts for organic reactions is their availability and easy preparation. Recently, BASF has commercialized under the name of Basolites/Basosiv a series of five MOFs having different metals and linkers (Basolite A100, C300, F300, Z1200 and Basosiv M050 or aluminum terephthalate MIL-53, copper trimesate HKUST-1, iron trimesate, zinc imidazolate or ZIF-8, and magnesium formate, respectively).^{12–18} Out of these materials, Fe(BTC) (BTC: 1,3,5-benzenetricarboxylate) has been reported to be a highly active catalyst for some reactions

requiring Lewis acidity, such as ring-opening of epoxides,¹⁹ acetalization of aldehydes,²⁰ methylation of amines,²¹ aldol condensation,²² aerobic oxidation of thiophenol to diphenylsulfide,²³ and benzylic oxidations by *tert*-butylhydroperoxide (TBHP)²⁴ and aerobic oxidation reactions catalyzed by *N*-hydroxyphthalimide-containing Fe(BTC) as catalysts.^{25–27}

In contrast to the other four commercially available MOFs, the structure of Fe(BTC) remains unknown due to its poor crystallinity. Interestingly, although chemical composition of commercial Fe(BTC) and synthetic MIL-100(Fe) is similar (both are constituted by Fe(III) and BTC, in fact), the structure, purity, counterion, or remaining solvent might differ. The mesoporous MIL-100(Fe) or $\text{Fe}_3\text{O}(\text{H}_2\text{O})_2((\text{CO}_2)_3\text{C}_6\text{H}_3)_2n\text{H}_2\text{O}$ is based on hybrid supertetrahedra built up from oxocentered trimers of iron(III) octahedra connected by trimesate anions.²⁸ The assembling of these hybrid supertetrahedra leads to a $Fd\bar{3}m$ (no. 227) zeotype structure, delimiting two types of mesoporous cages of free apertures of 25 and 29 Å, accessible through microporous

Received: June 4, 2012

Revised: July 24, 2012

Published: August 17, 2012

windows of 5.5 and 8.6 Å. In addition, MIL-100(Fe) solid possesses accessible coordinatively unsaturated metal sites (CUS) as well as interesting reduction properties.^{29,30}

Although in catalysis, to gain understanding on the reaction mechanism, the knowledge of the crystal structure (cavity dimensions, atomic distances, accessibility, etc.) is mandatory, the fact that MIL-100(Fe) is still not commercialized could make commercially available Fe(BTC) a preferred material for use, despite its unknown structure, which makes it difficult to rationalize its catalytic activity.

In this context, the comparison of both structural and compositional features and the catalytic activity of commercial Fe(BTC) with that of MIL-100(Fe) can serve to delineate the similarities and differences between these two materials, providing data concerning which of these two solids is the best performing catalyst for different reactions. Aimed at establishing the relative activity of commercial F300 and MIL-100(Fe), we have selected four representative reactions, two of them requiring Lewis acidity and another two that are oxidation reactions. In particular, we have selected two general transformations in organic chemistry, aldehyde acetalization and epoxide ring-opening reactions by methanol, that are typically catalyzed by metal halides and other Lewis acids.¹⁹ The oxidation reactions chosen were the benzylic oxidation of diphenylmethane (DPM) by TBHP and the aerobic oxidation of thiophenol. The results are of interest for the understanding of the role that defects [the case of Fe(BTC)] and structure stability [the case of MIL-100(Fe)] play in the catalytic activity, depending on the reaction type.

RESULTS AND DISCUSSION

While the transformation of DPM by TBHP involves large reagents and bulky transition states, a priori requiring larger pores size, the oxidation of thiophenol is much less demanding from a steric point of view. These four reactions have been already reported to be catalyzed by Fe(BTC), and they can serve to give a view of the relative catalytic activity of Fe(BTC) and MIL-100(Fe).^{20,23,24,26}

Physical characterization of Fe(BTC) and MIL-100(Fe). MIL-100(Fe) and Fe(BTC) exhibit different powder X-ray diffraction (PXRD) patterns, revealing a poor crystallinity for the Fe(BTC) solid (Supporting Information Figure S1). After outgassing both samples at 150 °C for 3 h, the broad trimesate bands observed by infrared spectroscopy (IR) at 1120 and 930 cm⁻¹ of the Fe(BTC) are consistent with the lower crystallinity of this sample. In addition, the intensity of the carbonyl band at 1745 cm⁻¹, twice higher in the Fe(BTC) than in MIL-100(Fe) solid, indicates the presence of an additional amount of extraframework BTC in its acid form, even after the outgassing procedure. Fe(BTC) also presents supplementary bands at 2960, 2935, and 2876 cm⁻¹ assigned to aliphatic CH groups. Table 1 displays the comparison of the composition and textural parameters of Fe(BTC) and MIL-100(Fe). The cubic structure MIL-100(Fe) shows a higher porosity with larger cavities; the Fe(BTC) possesses smaller particle size and a slightly lower C/Fe ratio (5.8 vs 6.4), which further support structural differences and the presence of impurities deduced from PXRD and IR, respectively (see Supporting Information Figures S1 and S2).

Catalytic Studies. The first studied reaction was the acetal formation of benzaldehyde and cinnamaldehyde to form selectively the corresponding dimethyl acetal in both cases. Conversion and selectivity for this reaction are very similar

Table 1. Comparison of the Textural Properties and Acidity of Fe(BTC) and MIL-100(Fe)

properties	Fe(BTC)	MIL-100(Fe)
metal ion	Fe	Fe
linker	BTC ^a	BTC ^a
iron mass content (%)	25 ^b	21
carbon mass content (%)	32 ^b	29
crystal structure	unknown	cubic <i>Fd3m</i>
S _{BET} (m ² g ⁻¹)	840	2200
pore dimension (Å)	21.7 ^c	25, 29 ^d
particle size (in EtOH) (μm)	5	15
Lewis acid	strong	strong
Brønsted acid	weak	absence

^aBTC: 1,3,5-benzenetricarboxylate. ^bPresence of nitrogen (0.3%) and sulfur (0.1%). ^cObtained from nitrogen adsorption measurements. ^dEstimated from its crystal structure.

between Fe(BTC) and MIL-100(Fe) for the two selected substrates (Table 2 and Figure 1). Interestingly, both solids also exhibit initial reaction rates very similar to the methanol-soluble homogeneous catalyst iron nitrate, which, however, deactivates giving lower conversion at final time.

In contrast to the above results, Fe(BTC) and MIL-100(Fe) catalyst perform remarkably different for the ring-opening of styrene oxide, leading to 2-methoxy-1-phenylethanol. In particular, it seems that for this reaction occurring via a S_N1 mechanism and requiring stronger acid sites than acetalization,²⁰ MIL-100(Fe) is notably less active than Fe(BTC) or iron nitrate. The results are given in Table 2.

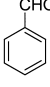
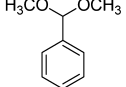
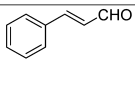
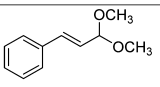
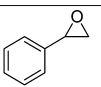
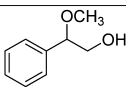
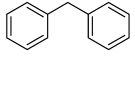
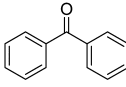
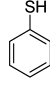
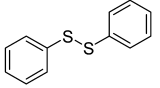
In contrast to the ring-opening of epoxide, the performance of MIL-100(Fe) for oxidation reactions was found better than that of Fe(BTC) (see Table 2). Particularly remarkable is the case of aerobic oxidation of thiophenol, leading to diphenyldisulfide. The time conversion plot for this aerobic oxidation promoted either by any of the two MOFs or by iron nitrate as homogeneous catalyst is shown in Figure 2. As can be seen there, for this reaction, MIL-100(Fe) is the best catalyst in terms of conversion. Again, Fe(III) MOFs exhibit much better catalytic activity than iron nitrate.

One of the main issues in heterogeneous catalysis is the leaching of metal sites from the solid catalyst to the liquid phase. To address this issue, in the present work, leaching tests were performed for all reactions, confirming that the process is heterogeneous and the reactions stop upon removal of Fe(BTC) or MIL-100(Fe) with negligible detection of iron in the solution, ruling out iron leaching from the hybrid solids to the liquid phase for the tested reactions.

Spectroscopic Characterizations of Acid and Redox Sites in Fe(BTC) and MIL-100(Fe). To better understand the different acid and redox catalytic activity of these two iron trimesates, acid strength and redox behavior^{29,30} of these solids were characterized by in situ IR and ⁵⁷Fe Mössbauer spectrometry.

Acidity was measured by adsorption of CD₃CN and pyridine. After activation at 150 °C for 3 h and CD₃CN adsorption, spectra of Fe(BTC) and MIL-100(Fe) display, in addition to the physisorbed species (band at 2265 cm⁻¹), a ν(CN) band at 2294 cm⁻¹ assigned to strong Lewis acid Fe sites (Figure 3). On MIL-100(Fe), the occurrence of an additional shoulder at 2307 cm⁻¹, confirmed on the spectrum after outgassing at 50 °C, reveals the presence of some Lewis sites having a stronger acidity than those of Fe(BTC). Thus, although both samples

Table 2. Catalytic Data Obtained for Fe(NO₃)₃ as Homogeneous Catalyst or in the Presence of Fe(BTC) and MIL-100(Fe) as Heterogeneous Catalysts for the Four Reactions under Study

Run	Substrate	Product	Catalyst	Time (h)	Conv. (%)
1 ^a			Fe(NO ₃) ₃ ·9H ₂ O	21	69
2			Fe(BTC)	21	84
3			MIL-100(Fe)	21	84
4 ^b			Fe(BTC)	24	69
5			MIL-100(Fe)	24	69
6 ^c			Fe(NO ₃) ₃ ·9H ₂ O	0.25	99
7			Fe(BTC)	1	99
8			MIL-100(Fe)	24	62
9 ^d			Fe(NO ₃) ₃ ·9H ₂ O	30	28
10			Fe(BTC)	30	6.5
11			MIL-100(Fe)	30	9
12 ^e			Fe(NO ₃) ₃ ·9H ₂ O	24	23
13			Fe(BTC)	24	64
14			MIL-100(Fe)	24	81

^aAcetalization conditions: benzaldehyde (0.300 mL), preactivated MOFs at 150 °C for 3 h (9 mg Fe(BTC) or 10 mg MIL-100(Fe) or 16 mg Fe(NO₃)₃·9H₂O), methanol (5 mL), 40 °C. ^bAcetalization (cinnamaldehyde): same as above except 0.250 mL of cinnamaldehyde. ^cStyrene oxide (0.250 mL), preactivated MOFs at 150 °C for 3 h (47 mg Fe(BTC) or 50 mg MIL-100(Fe) or 86 mg Fe(NO₃)₃·9H₂O), methanol (5 mL), 40 °C. ^dDPM (0.100 mL), preactivated MOFs at 150 °C for 3 h (9 mg Fe(BTC) or 10 mg MIL-100(Fe) or 16 mg Fe(NO₃)₃·9H₂O), 80% TBHP (0.075 mL), acetonitrile (5 mL), 70 °C. ^eThiophenol (0.250 mL), preactivated MOFs at 150 °C for 3 h (9 mg Fe(BTC) or 10 mg MIL-100(Fe) or 16 mg Fe(NO₃)₃·9H₂O), oxygen purged through balloon, acetonitrile (5 mL), 70 °C.

Fe(BTC) and MIL-100(Fe) exhibit strong Lewis acidity, the latter appears to be the strongest one.

The existence of strong acid sites on MIL-100(Fe) has been previously explained by the presence of fluorine in the neighborhood of Fe sites, which increases the acid strength by an electron-withdrawing effect.^{29,30} Regarding the intensity of the $\nu(\text{CN})$ band of coordinated species, it is one-third higher on MIL-100(Fe), indicating that the density of Lewis sites is

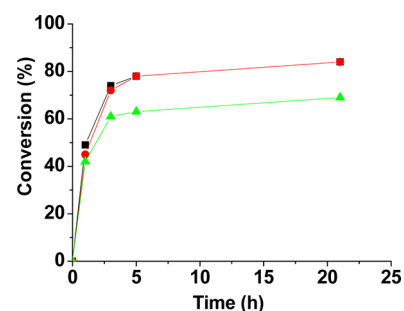


Figure 1. Time conversion plot for acetalization of benzaldehyde by iron nitrate (green triangles), Fe(BTC) (black squares), and MIL-100(Fe) (red circles). See Table 2 for reaction conditions.

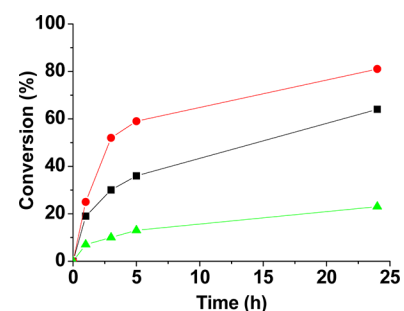


Figure 2. Time conversion plot for the aerobic oxidation of thiophenol to diphenyldisulfide catalyzed by iron nitrate (green triangles), Fe(BTC) (black square), and MIL-100(Fe) (red circles). See Table 2 for reaction conditions.

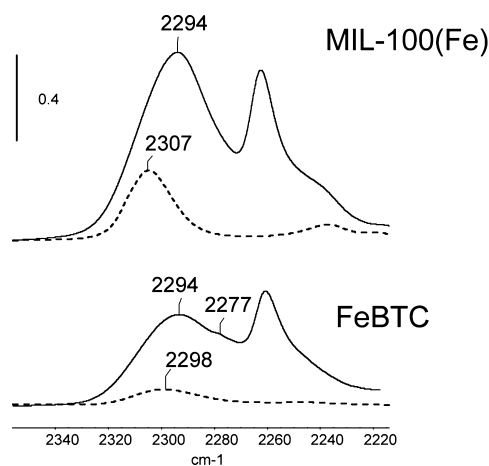


Figure 3. IR spectra of CD₃CN adsorbed on FeBTC and MIL-100(Fe) activated at 150 °C for 3 h. Solid line: spectra recorded under an equilibrium pressure of 70 Torr at room temperature. Dotted line: After evacuation at 50 °C. Spectra are normalized to the same amount of dried material (10 mg).

higher on this material compared with Fe(BTC). This result is confirmed by quantitative results obtained by pyridine adsorption, as presented thereafter.

Adsorption of pyridine on MIL-100(Fe) and Fe(BTC) leads to the observation of three bands at 1014, 1043, and 1070 cm⁻¹ (Figure 4a), previously assigned to the $\nu 1$, $\nu 12$, and $\nu 18$ modes, respectively, of pyridine coordinated on Fe³⁺ Lewis acid sites (we recall here that the usually monitored $\nu 8$ and $\nu 19$ pyridine modes are hindered by the carboxylate vibrations).^{29,32} On Fe(BTC), a $\nu 1$ band at 1007 cm⁻¹, related to the occurrence of a continuum absorption between 3000 and 1900 cm⁻¹

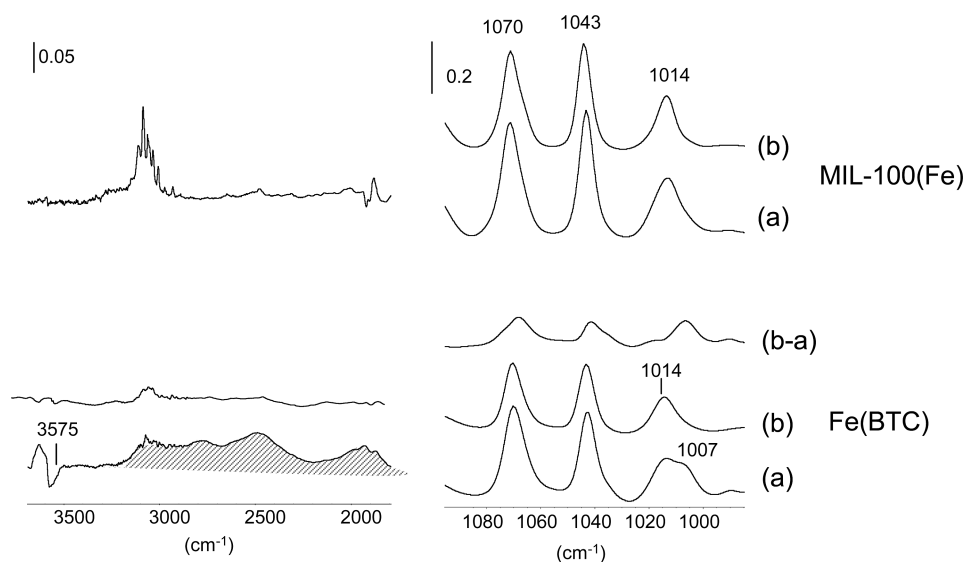


Figure 4. IR spectra of MIL-100(Fe) (top) and Fe(BTC) (bottom) activated at 150 °C for 3 h after adsorption of pyridine and followed by evacuation at room temperature (a) and at 100 °C (b). Spectra are normalized to the same amount of dried material (10 mg).

composed of three submaxima situated at about 2800, 2500, and 2000 cm^{-1} , reveals another type of adsorbed pyridine species. In solution, these spectral features are characteristic of strong hydrogen interactions between pyridine and acidic OH groups such as those of carboxylic acids.³¹ In Fe(BTC), such OH groups might be characterized by a $\nu(\text{OH})$ band at 3575 cm^{-1} (negative band in Figure 4a). This is confirmed after outgassing at 100 °C: the bands associated with H-bonded species are removed, and the 3575 cm^{-1} band is restored. As for the intensities of coordinated species, they are much less important on Fe(BTC). Considering the molar absorption coefficient of the 1050 cm^{-1} band ($0.5 \text{ cm} \cdot \mu\text{mol}^{-1}$) (as found on MIL-100(Al)),³² the concentration of Lewis acid sites has been quantified on both samples. They are equal to 2000 and 1100 $\mu\text{mol} \cdot \text{g}^{-1}$ for MIL-100(Fe) and Fe(BTC), respectively. These values correspond to about 40 and 30% of the total number of Fe atoms contained in these materials, respectively.

It has been previously observed that the presence of impurities such as carboxylic acid coordinated on metal sites decreases the concentration of Lewis acid sites.³² The higher amount of carboxylic impurities present on Fe(BTC) could explain the lower proportion of Fe Lewis acid sites on this material.

Taking in consideration the above IR results, although Fe(BTC) shows a lower number of weaker Lewis acid sites than MIL-100(Fe), its catalytic activity as a solid acid is surprisingly higher and does not appear to correlate with the density and strength of Lewis acid sites that are associated with exchangeable coordination positions of Fe^{3+} ions. Considering that acetalization and epoxide ring-opening are typical acid-catalyzed reactions, one can suggest tentatively that its higher catalytic activity could be related to the presence of additional weak Brønsted acid sites, evidenced by IR pyridine adsorption (Figure 4, Table 1). This fact, together with the smaller particle size of Fe(BTC) (Table 1) and the presence of free acid or unknown impurities Fe(BTC) could explain its higher acid catalytic activity.

In addition to the acid density and strength, the redox behavior of Fe(BTC) compared with MIL-100(Fe) was also evaluated. Previous experimental work based on IR and

Mössbauer spectrometry gave evidence that thermal activation can effect the reduction of Fe^{3+} into Fe^{2+} coordinatively unsaturated sites in MIL-100(Fe) (even if the reverse process was never evidenced).³⁰ Herein, we have also proceeded to establish the conditions for the reduction of Fe^{3+} to Fe^{2+} in Fe(BTC) compared with MIL-100(Fe). First, iron reduction was followed by IR spectroscopy by adsorption of NO. Room temperature NO adsorption on Fe(BTC) and MIL-100(Fe) samples activated at 150 °C (Figure 5) reveals a weak band

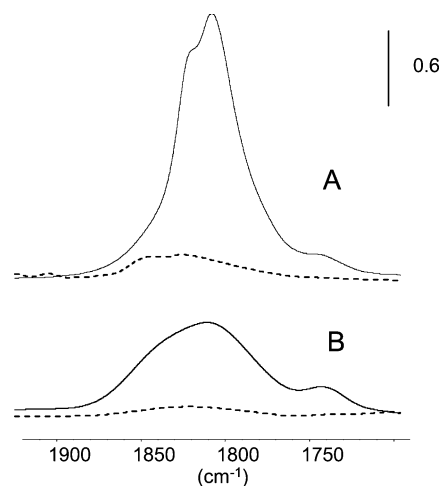


Figure 5. IR spectra of NO adsorbed at room temperature on MIL-100(Fe) (A) and Fe(BTC) (B) after outgassing 3 h at 150 °C (dotted line), 12 h at 250 °C (solid line), 12 h at 250 °C (solid line). Spectra are normalized to the same amount of dried material (10 mg).

centered at about 1815 cm^{-1} on both samples, indicating the presence of only a small amount of NO adsorbed on Fe^{2+} sites. After activation at 250 °C, the intensity of the 1815 cm^{-1} band increases, showing the creation of Fe^{2+} sites after the more severe thermal treatment. Its intensity is much higher on MIL-100(Fe), showing that the number of reducible Fe sites is more important in this sample, in agreement with Mössbauer spectroscopic results presented thereafter.

Mössbauer Spectrometry. ^{57}Fe Mössbauer spectra were first collected for samples under ambient conditions (atmosphere, pressure, and temperature) and then at $-196\text{ }^\circ\text{C}$ with large and small velocity range (12 and 2 mm/s, respectively; Supporting Information Figure S4). It is observed that no magnetic Fe species are detectable in both Fe(BTC) and MIL-100(Fe) samples, excluding thus the presence of iron oxide impurities in the sample. Asymmetrical pure quadrupolar features with broadened lines were observed, however, at both 27 and $-196\text{ }^\circ\text{C}$ (Figure 6 and Supporting Information

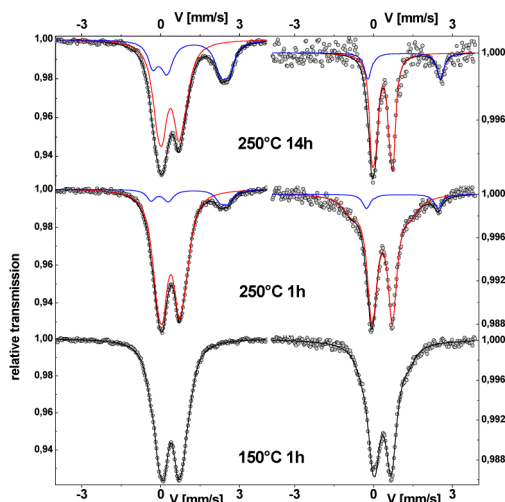


Figure 6. Mössbauer spectra of Fe(BTC) (left) and MIL-100(Fe) (right) recorded at $-196\text{ }^\circ\text{C}$ under vacuum after in situ annealing treatment using a cryofurnace at $150\text{ }^\circ\text{C}$ for 1 h, $250\text{ }^\circ\text{C}$ for 1 h, and $250\text{ }^\circ\text{C}$ for 14 h.

Figure S4). These features are consistent with a disordered environment of Fe ions in the octahedral units. The fitting model takes into consideration a distribution of quadrupolar splitting correlated with isomer shift. It is, however, important to emphasize that the values of both the hyperfine data and the ratio $\langle\Delta^2\rangle/\langle\Delta\rangle^2$ (about 1.40) suggest that Fe(BTC) is neither crystalline nor amorphous, but rather, disordered.³³ Interestingly, the mean values of isomer shift unambiguously indicate the presence of Fe^{3+} in Fe(BTC), excluding Fe^{2+} species. In the case of Fe(BTC), the hyperfine structure of Mössbauer spectra differ from room temperature and $-196\text{ }^\circ\text{C}$, in agreement with a change of local environment, probably originating from the departure of water molecules, as previously observed for MIL-100(Fe).³⁰

After these preliminary Mössbauer measurements at two temperatures, the Fe(BTC) sample was placed under vacuum ($\sim 5 \times 10^{-5}$ Torr) into a homemade cryofurnace, allowing thus the comparison of in situ Mössbauer measurements for Fe(BTC) at 77 K versus annealing temperature with the previously reported study for MIL-100(Fe).³⁰ Further changes are detected after subsequent annealing at 70 and $110\text{ }^\circ\text{C}$ for 1 h. Similar to MIL-100(Fe),³⁰ it was observed that the mean values of the isomer shift remain rather constant, whereas those of the quadrupolar splitting are significantly larger, suggesting important structural changes of the Fe environment resulting from the departure of water molecules.

Mössbauer spectra were then recorded at $-196\text{ }^\circ\text{C}$ after in situ annealing treatments at 150, 200, and $250\text{ }^\circ\text{C}$ for 1 h and then at $250\text{ }^\circ\text{C}$ for several cycles. Examples are given in Figure

6. These spectra clearly show the progressive appearance of a satellite line attributed to the increasing emergence of the Fe^{2+} component after outgassing both Fe(BTC) and MIL-100(Fe) samples at $250\text{ }^\circ\text{C}$, in agreement with IR data. The amount of Fe^{2+} for Fe(BTC) and MIL-100(Fe) is plotted as a function of time in Supporting Information Figure S5, assuming the same recoilless f factors for both solids. Remarkably, the amount of Fe^{2+} in Fe(BTC) progressively increases with time (from 12 to 44% at 1 and 30 h, respectively; Supporting Information Figure S5).

Although the amount of Fe^{2+} is higher in the Fe(BTC) than in the MIL-100(Fe) solid (34 vs 22 at % at $250\text{ }^\circ\text{C}$ 14 h), IR spectroscopy of Fe(BTC) after annealing at $250\text{ }^\circ\text{C}$ shows the appearance of new bands at 1805 (attributed previously to the formation of anhydride) and 1045 cm^{-1} and the disappearance of trimesate bands at 1120 and 930 cm^{-1} , indicating the degradation of the solid (Supporting Information Figure S3). IR data after treatment at $250\text{ }^\circ\text{C}$ are also consistent with the XRD data (Supporting Information Figure S1 recorded for this sample), that show a clear amorphization of the Fe(BTC). In contrast, MIL-100(Fe) did not show any evidence of degradation up to $280\text{ }^\circ\text{C}$ under similar conditions,³⁰ supporting the partial reduction of Fe^{3+} to Fe^{2+} without degradation at $250\text{ }^\circ\text{C}$. These facts might explain the better activity of MIL-100(Fe) on the oxidation reactions, since they will indicate an easy and likely reversible Fe^{3+} -to- Fe^{2+} change without destruction of the crystal structure.

CONCLUSIONS

While the commercial Fe(BTC) is the best catalyst for Lewis acid reactions because of its additional Brönsted acid sites, MIL-100(Fe) would be the best choice for oxidation reactions due to the presence of $\text{Fe}^{3+}/\text{Fe}^{2+}$ pairs, which seem to give rise to an interchange without compromising the crystal structure. The catalytic results provide, therefore, indirect evidence of the redox properties of the investigated material. These results point out the domain of possible applications for the commercially available Fe(BTC) in heterogeneous catalysis and open new possibilities concerning oxidation reactions by MIL-100(Fe). Overall, these results illustrate the importance of defects [the case of Fe(BTC)] and structure robustness [the case of MIL-100(Fe), in which (reversible) $\text{Fe}^{3+}/\text{Fe}^{2+}$ changes occur without damaging the crystal lattice] on the catalytic activity of MOFs, depending on the reaction type.

EXPERIMENTAL SECTION

All reagents, starting materials and Fe(BTC) were obtained commercially from Aldrich and were used as received. MIL-100(Fe) was synthesized by a hydrothermal method as reported by elsewhere.²⁸ Both solids were characterized by powder X-ray diffraction (PXRD), infrared (IR) and Mössbauer spectroscopies, thermogravimetric analysis (TGA), elemental analysis, and nitrogen adsorption porosimetry.

PXRD patterns have been collected in a Siemens D5000 diffractometer (radiation $\text{Cu K}\alpha$ $\lambda_{\text{Cu}} = 15406\text{ \AA}$, mode θ - 2θ) at room temperature. TGA was performed on a Perkin-Elmer Diamond TGA/DTA STA 6000 under O_2 atmosphere ($20\text{ mL}\cdot\text{min}^{-1}$) between room temperature and $600\text{ }^\circ\text{C}$ in an aluminum crucible (heating speed $2\text{ }^\circ\text{C}/\text{min}$) using 5–10 mg of hydrated products. Nitrogen adsorption isotherms were performed at $-196\text{ }^\circ\text{C}$ on a Belsorp Mini (Bel, Japan)

apparatus using nitrogen as the probing gas and outgassing the samples at 200 °C under dynamic vacuum for 16 h.

In situ IR experiments were performed on self-supported sample disks (2 cm² area, 7–10 mg cm⁻²) placed in a quartz cell equipped with KBr windows. A movable quartz sample holder allows adjusting the pellet in the infrared beam for spectra acquisition and displacing it into a furnace at the top of the cell for thermal treatments. The cell was connected to a vacuum line for evacuation (residual pressure = 10⁻³–10⁻⁴ Pa), calcination steps, and introduction of gases and vapors into the infrared cell. Transmission IR spectra were recorded in the 650–5600 cm⁻¹ range, with a 4 cm⁻¹ resolution, on a Nicolet Nexus spectrometer equipped with an extended KBr beam splitting device and a mercury cadmium telluride (MCT) cryodetector.

General Reaction Procedure. A 50 mL round-bottomed flask was charged with the required amount of catalyst and activated at 150 °C under air for 3 h. This preactivated catalyst was suspended in the appropriate solvent, and the corresponding substrate was added. A similar procedure was followed with iron nitrate as homogeneous catalyst, except that no activation step was performed. The reaction was stirred by heating at the required temperature and time. The reaction mixture was periodically analyzed by gas chromatography (GC). At the final reaction time, the reaction mixture was filtered. The mass balances of the recovered reaction mixture accounted for more than 97% of the initial substrate, as confirmed by GC using nitrobenzene as internal standard. In the case of oxidation reactions, the above procedure was followed, but TBHP was added or oxygen was purged with a balloon.

The percentage conversion, purity, and relative yields of the final products were determined using a Hewlett-Packard 5890 series II gas chromatograph with a FID detector and high-purity helium as the carrier gas. The products were identified by gas chromatography/mass spectrometry GC/MS using a Hewlett-Packard 6890 series spectrometer.

■ ASSOCIATED CONTENT

📄 Supporting Information

Five figures are provided as Supporting Information. This material is available free of charge via the Internet at <http://pubs.acs.org>.

■ AUTHOR INFORMATION

Corresponding Author

*Corresponding Author: hgarcia@qim.upv.es.

Notes

The authors declare no competing financial interest.

■ ACKNOWLEDGMENTS

Financial support by the Spanish Ministry of Science and Innovation (CTQ2009-11587, CTQ2010-18671, and Consolider MULTICAT) is gratefully acknowledged. This work has been funded in part by MACADEMIA (www.macademia-project.eu), a 4-year Large-Scale Integrating Collaborative Project funded by the European Community's Seventh Framework Programme (FP7/2007-2013) under Grant agreement No. 228862 (Nanosciences, Nanotechnologies, Materials and New Production Technologies Theme). M.D and A.V. thank G. Le Bars for assistance with infrared measurements.

■ REFERENCES

- (1) Farrusseng, D.; Aguado, S.; Pinel, C. *Angew. Chem., Int. Ed.* **2009**, *48*, 7502.
- (2) Lee, J. Y.; Farha, O. K.; Roberts, J.; Scheidt, K. A.; Nguyen, S. T.; Hupp, J. T. *Chem. Soc. Rev.* **2009**, *38*, 1450.
- (3) Corma, A.; Garcia, H.; Llabres i Xamena, F. X. *Chem. Rev.* **2010**, *110*, 4606.
- (4) Dhakshinamoorthy, A.; Garcia, H. *Chem. Soc. Rev.* **2012**, *15*, 5262–5284.
- (5) Férey, G. *Chem. Soc. Rev.* **2009**, *37*, 191.
- (6) Dhakshinamoorthy, A.; Alvaro, M.; Garcia, H. *Catal. Sci. Technol.* **2011**, *1*, 856–867.
- (7) Natarajan, S.; Mahata, P. *Chem. Soc. Rev.* **2009**, *38*, 2304.
- (8) Keeffe, M. O.; Peskov, M. A.; Ramsden, S. J.; Yaghi, O. M. *Acc. Chem. Res.* **2008**, *41*, 1782.
- (9) Clearfield, A. *Prog. Inorg. Chem.* **1998**, *47*, 371.
- (10) Reed, C. A. *Acc. Chem. Res.* **2005**, *38*, 215–216.
- (11) Dhakshinamoorthy, A.; Alvaro, M.; Corma, A.; Garcia, H. *Dalton Trans.* **2011**, *40*, 6344–6360.
- (12) Sigma Aldrich <http://www.basf.com> - <http://www.sigmaaldrich.com>
- (13) Mueller, U.; Schubert, M.; Teich, F.; Puetter, H.; Schierle-Arndt, K.; Pastre, J. *J. Mater. Chem.* **2006**, *16*, 626–636.
- (14) Cavenati, S.; Grande, C. A.; Rodrigues, A. E.; Kiener, C.; Muller, U. *Ind. Eng. Chem. Res.* **2008**, *47*, 6333–6335.
- (15) Czaja, A. U.; Trukhan, N.; Müller, U. *Chem. Soc. Rev.* **2009**, *38*, 1284.
- (16) Müller, U.; Lobree, L.; Hesse, M.; Yaghi, O. M.; Eddaoudi, M. *Shaped Bodies Containing Metal-Organic Frameworks*; US 2003/0222023 A1, US 10/157182, 2003.
- (17) Müller, U.; Lobree, L.; Hesse, M.; Yaghi, O. M.; Eddaoudi, M. *Shaped Bodies Containing Metal-Organic Frameworks*, BASF; US 6893564 B2, US 10/157182, 2005.
- (18) Hesse, M.; Mueller, U.; Yaghi, O. M. *Shaped Bodies Containing Metal-Organic Frameworks*; US 20090155588, 2009.
- (19) Dhakshinamoorthy, A.; Alvaro, M.; Garcia, H. *Chem.—Eur. J.* **2010**, *16*, 8530–8536.
- (20) Dhakshinamoorthy, A.; Alvaro, M.; Garcia, H. *Adv. Synth. Catal.* **2010**, *352*, 3022–3030.
- (21) Dhakshinamoorthy, A.; Alvaro, M.; Garcia, H. *Appl. Catal. A* **2010**, *378*, 19–25.
- (22) Dhakshinamoorthy, A.; Alvaro, M.; Garcia, H. *Adv. Synth. Catal.* **2010**, *352*, 711–717.
- (23) Dhakshinamoorthy, A.; Alvaro, M.; Garcia, H. *Chem. Commun.* **2010**, *46*, 6476–6478.
- (24) Dhakshinamoorthy, A.; Alvaro, M.; Garcia, H. *J. Catal.* **2009**, *267*, 1–4.
- (25) Dhakshinamoorthy, A.; Alvaro, M.; Garcia, H. *ChemCatChem* **2010**, *2*, 1438–1443.
- (26) Dhakshinamoorthy, A.; Alvaro, M.; Garcia, H. *Chem.—Eur. J.* **2011**, *17*, 6256–6262.
- (27) Dhakshinamoorthy, A.; Alvaro, M.; Garcia, H. *ACS Catal.* **2011**, *1*, 836–840.
- (28) Horcajada, P.; Surblé, S.; Serre, C.; Hong, D.-Y.; Seo, Y.-K.; Chang, J.-S.; Grenèche, J.-M.; Margiolaki, I.; Férey, G. *Chem. Commun.* **2007**, 2820.
- (29) Leclerc, H.; Vimont, A.; Lavalley, J. C.; Daturi, M.; Wiersum, A. D.; Llwelllyn, P. L.; Horcajada, P.; Férey, G.; Serre, C. *Phys. Chem. Chem. Phys.* **2011**, *13*, 11748.
- (30) Yoon, J. W.; Seo, Y.-K.; Hwang, Y. K.; Chang, J.-S.; Leclerc, H.; Wuttke, S.; Bazin, P.; Vimont, A.; Daturi, M.; Bloch, E.; Llwelllyn, P. L.; Horcajada, P.; Serre, C.; Grenèche, J.-M.; Rodrigues, A. E.; Férey, G. *Angew. Chem., Int. Ed.* **2010**, *49*, 5949.
- (31) Odínokov, S. E. *Spectrochim. Acta* **1975**, *32A*, 1355.
- (32) Volkringer, C.; Leclerc, H.; Lavalley, J.-C.; Loiseau, T.; Férey, G.; Daturi, M.; Vimont, A. *J. Phys. Chem. C* **2012**, *116*, 5710.
- (33) López-Herrera, M. E.; Grenèche, J. M.; Varret, F. *Phys. Rev. B* **1982**, *28*, 4944–4948.